AFRL-AFOSR-VA-TR-2016-0166

Phase-Sensitive Control Of Molecular Dissociation Through Attosecond Pump/Strong-Field Mid-IR Probe Spectroscopy

Jeffery Moses
MASSACHUSETTS INSTITUTE OF TECHNOLOGY

04/15/2016
Final Report

Air Force Research Laboratory
AF Office Of Scientific Research (AFOSR)/ RTB1
Arlington, Virginia 22203
Air Force Materiel Command

REPORT DOCUMENTATION PAGE

Form Approved
OMB No. 0704-0188

1. REPORT DATE *(DD-MM-YYYY)*	2. REPORT TYPE	3. DATES COVERED *(From - To)*
19-04-2016	Final Performance	01 Apr 2012 to 30 Nov 2015

4. TITLE AND SUBTITLE
Phase-Sensitive Control Of Molecular Dissociation Through Attosecond Pump/Strong-Field Mid-IR Probe Spectroscopy

5a. CONTRACT NUMBER

5b. GRANT NUMBER
FA9550-12-1-0080

5c. PROGRAM ELEMENT NUMBER
61102F

6. AUTHOR(S)
Jeffery Moses

5d. PROJECT NUMBER

5e. TASK NUMBER

5f. WORK UNIT NUMBER

7. PERFORMING ORGANIZATION NAME(S) AND ADDRESS(ES)
MASSACHUSETTS INSTITUTE OF TECHNOLOGY
77 MASSACHUSETTS AVE
CAMBRIDGE, MA 02139-4301 US

8. PERFORMING ORGANIZATION REPORT NUMBER

9. SPONSORING/MONITORING AGENCY NAME(S) AND ADDRESS(ES)
AF Office of Scientific Research
875 N. Randolph St. Room 3112
Arlington, VA 22203

10. SPONSOR/MONITOR'S ACRONYM(S)
AFRL/AFOSR RTB1

11. SPONSOR/MONITOR'S REPORT NUMBER(S)
AFRL-AFOSR-VA-TR-2016-0166

12. DISTRIBUTION/AVAILABILITY STATEMENT
A DISTRIBUTION UNLIMITED: PB Public Release

13. SUPPLEMENTARY NOTES

14. ABSTRACT
Our program developed key technologies for strong-field and attosecond physics, specifically towards the goal of sequentially controlling
ionization and dissociation steps in the H2+ molecule using tightly synchronized few-fs EUV and few-cycle mid-IR pulses. We developed a cryocooled
laser and optical parametric chirped pulse amplification based light pulse architecture, producing, by high harmonic generation, a 16-18 eV
isolated single-femtosecond EUV pulse source, and by adiabatic difference frequency generation and optical parametric amplification, octavespanning
energetic mid-IR pulses at 2.6 and 6 micron wavelengths. In addition, we developed improvements to the FROG-CRAB attosecond EUV
pulse characterization method to aid precision attosecond spectroscopy experimentation, and a two-color EUV/mid-IR pump probe ion
spectroscopy system, employing coherent wavelength multiplexing for tight synchronization between optical pulses, an actively stabilized Mach-
Zender interferometer for scanning the delay between these pulses under vacuum, and a vacuum target chamber allowing the sequential use of
electron and ion time-of-flight spectrometers for in situ EUV pulse characterization and ion spectroscopy of strong-field molecular dissociation
dynamics. The scalability of this system in average power and repetition frequency will allow for a powerful strong-field physics platform.

15. SUBJECT TERMS
attosecond, molecular dissociation

16. SECURITY CLASSIFICATION OF:			17. LIMITATION OF ABSTRACT	18. NUMBER OF PAGES	19a. NAME OF RESPONSIBLE PERSON
a. REPORT	b. ABSTRACT	c. THIS PAGE			PARRA, ENRIQUE
Unclassified	Unclassified	Unclassified	UU		19b. TELEPHONE NUMBER *(Include area code)* 703-696-8571

FINAL PROGRESS SUMMARY

To: technicalreports@afosr.af.mil

Subject: Final Progress Statement to Dr. Enrique Parra

Contract/Grant Title: Phase-sensitive control of molecular dissociation through attosecond pump/strong-field mid-IR probe spectroscopy

Contract/Grant #: FA9550-12-1-0080

Reporting Period: 1 April 2012 to 30 November 2015

Abstract

The overarching goal of our program was to develop a novel laser and ion spectroscopy system and to use it for the study of strong-field light-matter interactions in the H2 molecule, with molecular ionization and dissociation timed precisely by means of synchronized few-fs EUV and few-cycle mid-IR pulses. This scheme is predicted to allow synchronization of a bound vibrational wavepacket oscillation cycle with a mid-IR electromagnetic field cycle. While our laser system was too low in EUV flux to study the dissociation physics of the H2 molecule in the two-color pulse scheme (upgrade to a laser repetition rate of $\geq$ 10 kHz will be necessary), our efforts produced advances, some major, in several core technologies that can be used for such experiments in the future. These technologies include

- **Two-color driven (EUV/mid-IR) ion spectroscopy**: we designed an interferometer combining EUV and mid-IR light pulses, stable to within a fraction of the mid-IR light field period, with a H2 molecular gas target at the aperture of an ion time-of-flight (TOF) spectrometer for molecular ion spectroscopy, an electron time-of-flight (TOF) spectrometer for attosecond pulse characterization, and an EUV spectrometer for EUV light pulse spectral characterization, all accessible while the system remains under vacuum.

- **Low photon energy (16-18 eV) isolated single-femtosecond EUV pulse generation**: combining the use of low ionization threshold gas, an annual near-IR drive beam, polarization gating, and spectral filtering, we engineered a source of isolated EUV light pulses covering the narrow range of frequencies allowing excitation of H2 to bound H2+ with a duration short enough (2.6 fs) to last a fraction of a bound H2+ vibrational wavepacket cycle. This is a first source of isolated EUV pulses in this energy range and at close to transform limited duration, and we expect our results will inform the approaches used by attosecond and photoemission spectroscopy researchers in the future. Furthermore, we improved the FROG-CRAB EUV pulse characterization method by means of a new algorithm allowing increased accuracy that will be valuable generally for attosecond spectroscopy, especially in the low-photon energy range, where the state-of-the-art approach can be plagued by significant systematic errors.

- **Few-cycle, intense, 2.6- and 6-micron mid-IR pulse generation**: combining a novel nonlinear optical approach for coherent octave-spanning mid-IR seed pulse generation

(adiabatic frequency conversion) with novel nonlinear optical materials for mid-IR OPA (ZGP and CSP), and using our few-cycle 2-micron pulse source as the OPA pump, we demonstrated octave-spanning intense mid-IR pulses centered in the 5-6 micron range. These pulses can drive strong-field dissociation synchronized to the vibrational frequency of H2+. The technologies demonstrated here are major advances that will boost strong-field physics in the mid-IR range, an area of current interest by the AFOSR and DoD.

- **High-energy coherent synthesis of few-cycle near-IR and mid-IR light pulse sources**: Using a cryo-Yb:YAG picoseond pump laser we scaled both 800-nm and 2-micron OPCPA systems in our pulse synthesizer to produce few-cycle, sub-mJ-energy pulses. These pulses can be coherently locked by means of the coherent wavelength multiplexing method to within a small fraction of the mid-IR optical period. We improved the picoseond cryo-Yb:YAG laser amplifier technology to be superior in stability, duration, and pulse energy. These improvements to OPCPA technology are major advances for the field.

Together, these technologies represent a significant step forward for attosecond and strong-field spectroscopy, employing a laser technology suitable for high average power and precisely shaped two-color pulse sequences to be used for control of atoms and molecules along both electronic and vibrational degrees of freedom.

List of milestones reached

Ion spectroscopy

1. Designed and implemented an ion-time-of-flight (TOF) spectrometer and a new vacuum chamber for combining ion TOF, electron TOF, and photon spectroscopy of strong-field dissociation. Incorporated an acceleration scheme for H2 gas fragments.
2. Implemented a hydrogen gas line and verified generation of H2+ and H+ ions by multiphoton ionization and/or strong-field dissociation in an intense IR field, and by direct photoionization by attosecond EUV pulse trains.

EUV/Attosecond pulse generation

3. Verified operation of our home-built attosecond pulse diagnostic (FROG-CRAB method) by characterization of attosecond pulse trains.
4. Completed construction of a hollow-core fiber compressor and dispersion management system as a few-cycle 800-nm driving source test bed for optimizing isolated EUV pulse generation.
5. Investigated low-energy EUV harmonic generation by using non-traditional molecular gases for HHG with low ionization threshold. Confirmed high-flux 11-th harmonic generation for pumping H2 gas in the 16-18 eV energy band required to produce bound H2+.
6. Improved the FROG-CRAB retrieval algorithm used for characterization of the 1-fs EUV pulse amplitude and phase. The central momentum approximation in standard FROG-CRAB and the assumption of a flat dipole transmission matrix element (DTME) add significant errors to the reconstruction of EUV pulses at low photon energy, as used in this program. We employed what we call the “Volkov transform generalized projections algorithm” to

circumvent these bandwidth restrictions of FROG-CRAB, while still maintaining the ability to reconstruct both the attosecond pulse and an arbitrary long-wavelength streak waveform.

7. Implemented polarization gating of high harmonic generation, thereby successfully reducing the temporal emission width to the equivalent of 1 to 2 half-cycles of the 800-nm driving pulse. Using our FROG-CRAB EUV characterization device, we measured a duration of 2.6 fs, marginally short enough for selective ionization of H2 to bound H2+ within a fraction of the 7.5-fs vibrational half-period of H2+ for two-color experiments. However, their flux is too low for ion-counting experiments to be completed on a day-long timescale.

5-micron pulse generation

8. Generated a coherent 2-5 micron (octave-spanning) spectrum by adiabatic difference frequency generation using a lithium niobate crystal, to be used as a seed laser for the 5-micron optical parametric amplifier (OPA).
9. Demonstrated compressibility of the mid-IR seed pulses down to 1.1-cycle duration.
10. Designed a mid-IR OPA based on ZGP and CSP crystals, instead of the AGGS originally proposed in our program, and verified an octave-spanning gain bandwidth around 5-micron wavelength when pumped by our few-cycle 2-micron OPCPA pulses from the pulse synthesizer.

Multiplexed laser system development

11. To allow multi-hour operation, improved the stability of the optical parametric chirped pulse amplifier (OPCPA) wavelength multiplexer through shortening of path lengths and implementation of beam pointing stabilization of the OPCPA pump laser (reducing peak-to-peak deviation of beam location at the OPA crystal from 500 microns over 30 minutes to 50 microns over 2 hours).
12. Increased the 800-nm OPCPA bandwidth to support a 7-fs transform-limited pulse (improved from 9-fs) for aiding isolated attosecond pulse generation.
13. Implemented cryo-Yb:YAG pumped power amplifier stages in the 2-micron and 800-nm OPCPA systems, obtaining 0.6 mJ, 10-fs pulses (7 fs transform limit) and 21-fs, 300-μJ pulses, respectively.
14. Identified a bistability issue in the cryo-Yb:YAG regenerative amplifier, and significant energy and beam-pointing fluctuations in the cryo-Yb:YAG pump system overall (despite a major effort to reduce these during year 2). Making the optical system stable and robust and appropriate for day-long spectroscopy experiments required an overhaul of the pump amplifier chain. We replaced the home-built cryo-Yb:YAG regenerative amplifier with a commercial room temperature Yb:KYW regenerative amplifier. To make up for the lower gain, we also needed to double the number of passes in the two cryo-Yb:YAG power amplifiers. The result was a dramatically improved amplifier chain, with 70 mJ/pulse before compression and a shorter pulse duration of 8 ps, due to the elimination of strong gain narrowing that was characteristic of the cryo-Yb:YAG regenerative amplifier. Energy stability was improved to 1.5% r.m.s shot-to-shot.

Archival publications during reporting period:

1. K.-H. Hong, C.-J. Lai, V.-M. Gkortsas, S.-W. Huang, J. Moses, E. Granados, S. Bhardwaj, and F. X. Kärtner, "High-harmonic generation in Xe, Kr, and Ar driven by a 2.1-μm source: high-harmonic spectroscopy under macroscopic effects," Phys. Rev. A **86**, 043412 (2012).

2. H. Suchowski, P. R. Krogen, S.-W. Huang, F. X. Kärtner, and J. Moses, "Octave-spanning coherent mid-IR generation via adiabatic difference frequency conversion," Opt. Express **21**, 28892-28901 (2013).

3. K.-H. Hong, C.-J. Lai, J. Siqueira, P. Krogen, J. Moses, L. C.-L. Chang, G. J. Stein, L. E. Zapata, and F. X. Kärtner "Multi-mJ, kHz, 2.1-μm optical parametric chirped-pulse amplifier and high-flux soft X-ray high-harmonic generation," Opt. Lett. 39, 3145 (2014).

4. S. Carbajo, E. Granados, D. Schimpf, A. Sell, K.-H. Hong, J. Moses, and F. X. Kärtner, "Efficient generation of ultra-intense few-cycle radially polarized laser pulses," Opt. Lett. 39, 2487-2490 (2014).

5. C. Manzoni, O. D. Mücke, G. Cirmi, S. Fang, J. Moses, S.-W. Huang, K.-H. Hong, G. Cerullo, and F. X. Kärtner, "Coherent pulse synthesis: towards sub-cycle optical waveforms," Laser & Photon. Rev. 9, 129 (2015).

6. C.-L. Chang, P. Krogen, H. Liang, G. J. Stein, J. Moses, C.-J. Lai, J. P. Siqueira, L. E. Zapata, F. X. Kärtner, and K.-H. Hong, "Multi-mJ, kHz, ps deep-ultraviolet source," Opt. Lett. 40, 665 (2015).

7. C.-L. Chang, P. Krogen, K.-H. Hong, L. E. Zapata, J. Moses, A.-L. Calendron, H. Liang, C.-J. Lai, G. J. Stein, P. D. Keathley, G. Laurent, and F. X. Kärtner, "High-energy, kHz, picosecond hybrid Yb-doped chirped-pulse amplifier," Opt. Express 23, 10132 (2015).

8. C.-J. Lai, K.-H. Hong, J. P. Siqueira, P. Krogen, C.-L. Chang, G. J. Stein, H. Liang, P. D. Keathley, G. Laurent, J. Moses, L. E. Zapata, and F. X. Kärtner, "Multi-mJ mid-infrared kHz OPCPA and Yb-doped pump lasers for tabletop coherent soft x-ray generation," J. Opt. 17, 094009 (2015).

9. P. D. Keathley, S. Bhardwaj, J. Moses, G. Laurent, and F. Kaertner, "Volkov Transform Generalized Projection Algorithm for Attosecond Pulse Characterization," New J. of Physics (Submitted, 2016).

<u>Conference papers publishing work accomplished by this grant, not yet submitted to archival journals</u>:

1. P. Krogen, H. Suchowski, G. J. Stein, F. Kärtner, and J. Moses, "Tunable and Near-Fourier-limited Few-Cycle Mid-IR Pulses via an Adiabatically Chirped Difference Frequency Grating," in CLEO: 2014, OSA Technical Digest (online) (Optical Society of America, 2014), paper SM3I.5.

2. P. R. Krogen, H. Suchowski, G. J. Stein, F. X. Kärtner, and J. Moses, "Tunable Few-Cycle

Mid-IR Pulses towards Single-Cycle Duration by Adiabatic Frequency Conversion," in 19th International Conference on Ultrafast Phenomena, OSA Technical Digest (online) (Optical Society of America, 2014), paper 08.Tue.D.6.

3. P. Krogen, H. Suchowski, H. Liang, F. X. Kaertner, and J. Moses, "Toward Multi-Octave Pulse Shaping by Adiabatic Frequency Conversion," in CLEO: 2015, OSA Technical Digest (online) (Optical Society of America, 2015), paper SW1O.3.

4. P. Krogen, H. Suchowski, H. Liang, K.-H. Hong, F. Kärtner, J. Moses, "Generation of a Single-Cycle Pulse at 2.6 μm using Adiabatic Difference Frequency Generation", to be published in proceedings of International Conference on Ultrafast Phenomena (UP) 2016, Tucson, Arizona.

5. H. K. Liang, P. Krogen, K. Zawilski, P. G. Schunemann, T. Lang, U. Morgner, F. Kärtner, J. Moses, and K. Hong, "Octave-Spanning 6-μm OPA Pumped by 2.1-μm OPCPA," in High-Brightness Sources and Light-Driven Interactions, OSA technical Digest (online) (Optical Society of America, 2016), paper MS4C.1.

6. P. Krogen, H. K. Liang, K. Zawilski, P. G. Schunemann, T. Lang, U. Morgner, J. Moses, F. Kärtner, and K. Hong, "Octave-spanning 1.5-optical-cycle 6.5-μm OPA pumped by 2.1-μm OPCPA," to be published in CLEO: 2016, OSA Technical Digest (2016).

Details of milestones reached

I. Ion spectroscopy

To conduct an experiment requiring a precisely characterized and timed sequence of single-femtosecond EUV and few-cycle mid-IR pulses passing by an ion time-of-flight (TOF) spectrometer for kinetic-energy-release (KER) ion spectroscopy of molecular gases, we developed a vacuum and instrumentation system as depicted in Fig. I.1. The system is a modified FROG-CRAB EUV generation and pulse characterization setup funded through DARPA, AFOSR, and the Center for Free Electron Lasers (Hamburg). For the purpose of this project, we have implemented an ion time-of-flight (TOF) spectrometer together with a molecular gas target vacuum chamber allowing switching between use of the ion TOF and an electron TOF while under high vacuum. This allows the system's two purposes to be performed in sequence during an ion spectroscopy experiment. First, the system is used to optimize attosecond/EUV pulse generation using polarization gating, EUV spectral filtering, and FROG-CRAB characterization. Second, it is used to perform the dual color spectroscopy, in which the EUV pulses are combined with tightly synchronized mid-IR light pulses.

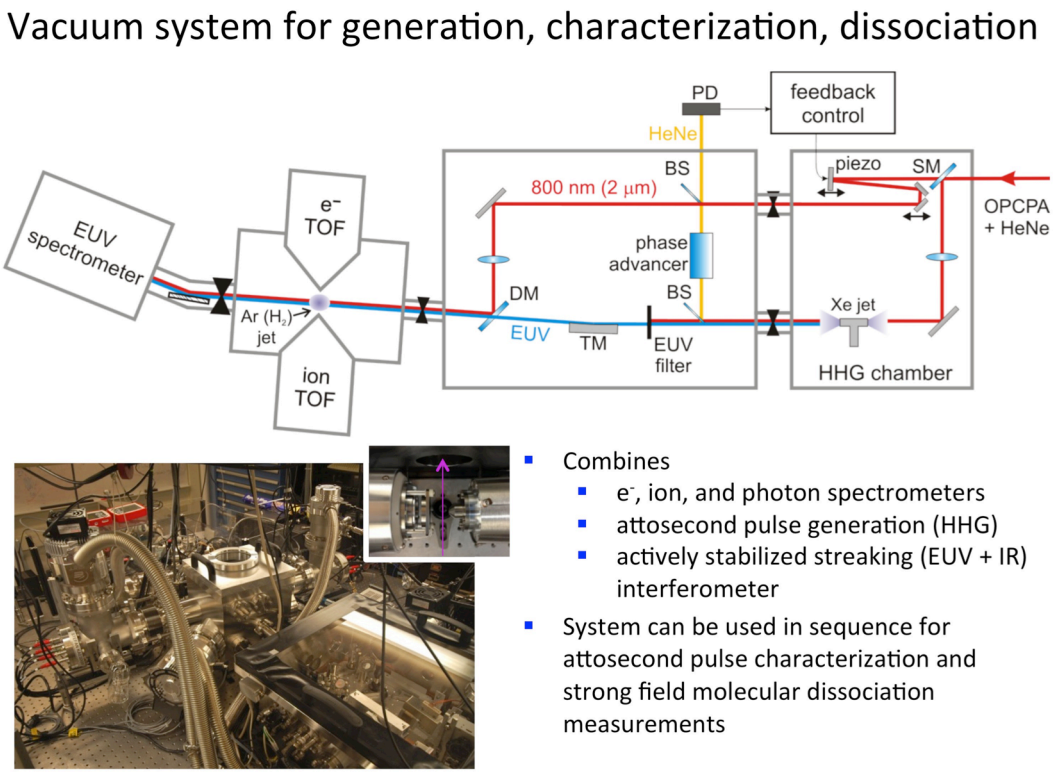

Fig. I.1 Schematic of ion spectroscopy with two color (EUV + mid-IR) laser fields, as constructed at MIT for this project. *Top:* layout of vacuum chambers. *From right to left:* 1) double chamber housing interferometer for attosecond streaking with dual purpose of FROG CRAB characterization of attosecond/EUV pulses and precisely timed delivery of EUV/mid-IR double-pulse train for ion spectroscopy; 2) chamber housing electron and ion time-of-flight (TOF) spectrometers; 3) Rowland-circle type EUV spectrometer. PD = photodiode, BS = beamsplitter, DM = drilled mirror, TM = toroidal mirror, SM = specialized mirror. *Bottom left*: photograph of vacuum chambers. Inset shows direction of EUV/mid-IR beams across target area, set between ion and electron TOF apertures.

In both cases, infrared pulses from the laser system arrive into the vacuum apparatus from the right-hand side. The first component is a specialized mirror (SM). When the system is used for the optimization of EUV pulse generation this mirror is a custom, broadband gold beamsplitter used to split 870-nm pulses into a HHG drive and a near-IR streaking beam. In this case, EUV pulses generated in a pulsed noble gas jet are focused by a 86° grazing incidence toroidal mirror (TM) and recombined with the near-IR streaking beam with a drilled mirror (DM). The two beams are focused into an Ar gas jet, where the near-IR beam imparts delay-dependent momentum shifts on the photoelectrons generated by the EUV pulse. The electron energy spectrum collected by the e- TOF spectrometer allows FROG-CRAB characterization of the EUV pulse amplitude and phase. Alternatively, when the system is used for dual-color spectroscopy, the gold beamsplitter is replaced by an ITO-coated beamsplitter used to separate the near-IR and mid-IR pulses. The near-IR pulse is directed to the HHG gas jet for EUV pulse generation, as before, and the mid-IR pulse is directed along the streaking beam path for variable delay with the HHG pulse, once recombined as before using the DM. These two beams are focused into an H_2 gas jet, where the EUV beam ionizes the molecules and the mid-IR beam imparts a delay-dependent coupling of the bound and dissociative electronic potentials of the H_2^+ molecular ion. If dissociation occurs, H^+ ions are accelerated into the ion TOF by means of a

charged metal plate on the opposite side of the ion TOF aperture, allowing detection of the KER of the protons at the time of dissociation.

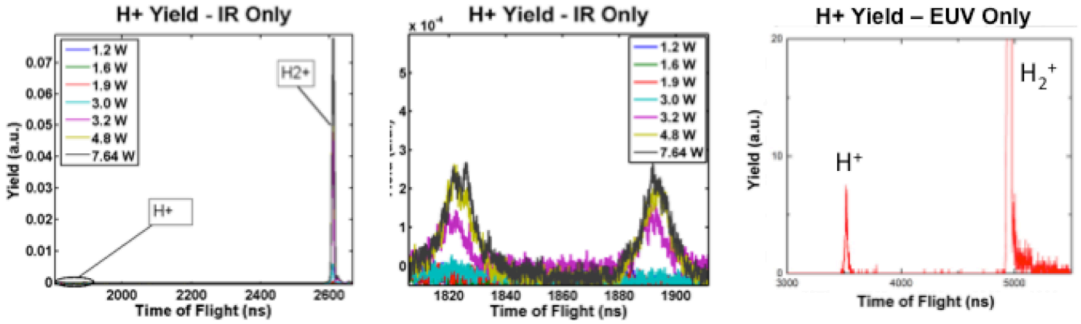

Fig. I.2. Ion TOF traces under influence of near-IR (left) and EUV (right) pulses only, using the ion spectroscopy setup described in Fig. I.1. For IR only, a strong enough pulse intensity results in sequential ionization and dissociation of H2 to produce protons of varying kinetic energy. A detailed look at the TOF trace corresponding to H+ arrival times (middle) shows two pulses. These correspond to protons initially moving away and toward the TOF, respectively. The symmetry of this trace allows calculation of the KER, i.e., the kinetic energy of the protons upon release from the dissociated H2+ molecule. For EUV only, in this case the photon energies cover a range suitable for ionization to both ground and excited H2+ states, thus both H+ and H2+ peaks can be seen. A large part of our effort was devoted to creating an isolated EUV pulse source covering the 16-18 eV range only (see Section II), thus allowing ionization of H2+ without the creation of excited (dissociative) molecular ions. (Note, different accelerating potentials were used for the IR and EUV measurements, resulting in differing times of flight for the same ion species.)

A system of bellows and movable TOF mounts, using lockable bearing carriages and guide rails, allowed us to place the ion and electron TOF spectrometers flanking a target gas jet to be used sequentially. The experimental procedure, carried out under vacuum, works as follows. First, the electron TOF is placed adjacent to the target and optimized in position using positioning bolts. HHG and polarization gating setups (see section II for details) are optimized in first pass using the EUV spectrometer. Then, using a piezo-controlled stage to delay the arrival of the IR streaking beam, the electron TOF is used to measure the time-dependent momenta of electrons removed from an Ar gas target under the combined influence of EUV pulse and IR streaking pulse. The resulting FROG-CRAB spectrogram is used to finely tune the polarization gating used for isolated EUV pulse generation. Third, using the positioning bolts, the electron TOF spectrometer is moved away from the gas target while the ion TOF spectrometer is moved towards it, until the gas jet is placed between the ion TOF entrance aperture and the acceleration plate. Finally, the Ar gas is replaced by H2, and the piezo-controlled stage is used to control the relative delay between isolated EUV and mid-IR pulses for strong-field dissociation measurements. Figure I.2 shows ion TOF traces after illumination by either IR or EUV pulses. In both cases, peaks corresponding to H+ and H2+ ions can be detected. As explained in Section II, we have developed an EUV pulse source to cover the 16-18 EUV photon range only, restricting the EUV pulses to ionize H2 and produce bound H2+ molecules only. The H+ dissociation yield due to two-color (EUV + IR) fields can then be isolated.

The Mach-Zender interferometer used to control the optical path length difference between EUV and IR beams is stabilized using a HeNe-based feedback loop superimposed on a majority of the beam path taken by the drive and streak beams. Using polarization optics (“phase advancer”), the phase of one arm of the HeNe interferometer can be adjusted continuously in one direction with high precision. With the feedback loop active, a timing jitter less than 250-as

r.m.s. is obtained. The optical period of 2.1-μm light is 7 fs. Thus, the correspondence between EUV and mid-IR pulse arrival times are reproduced with each laser shot to λ/35 precision.

II. EUV/Attosecond pulse generation

A. Generation of Isolated, Low-Energy EUV Pulse

Of paramount importance to exciting and studying the dissociation dynamics in H2 is the development of an isolated pulse of EUV photons in the appropriate energy range. In our case, the ideal energy range was between 16-18 eV in order to maximize the generation of oscillating (bound) H_2+ states. A direct route to generating isolated pulses was to first continue the development of our hollow core fiber (HCF) compressor front-end for our commercial, 35 fs, 800 nm titanium sapphire system. While we had used this system to generate pulses down to 8 fs FWHM [1], we had yet to generate high harmonics with it. To start, we upgraded our HHG generation system with a custom polarization gating setup to demonstrate that we could use the Ti:Sapph+HCF source to generate both harmonics and continuum spectra as others have demonstrated with similar systems. The results are shown in Fig. II.1.

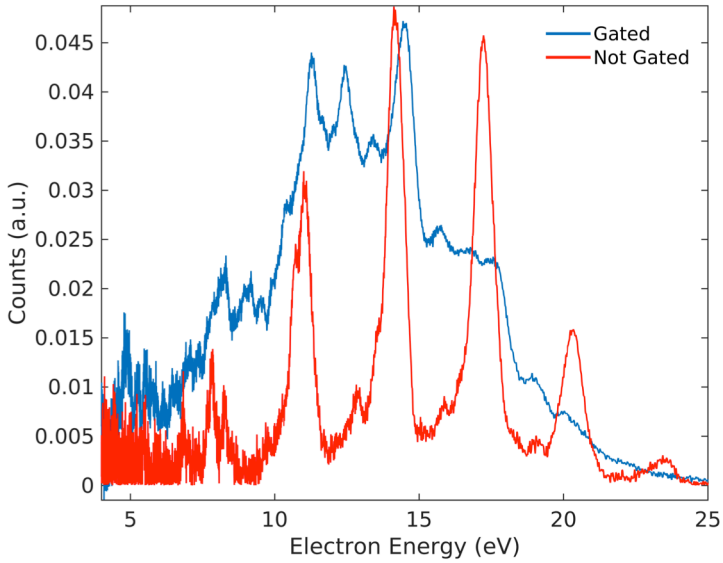

Fig. II.1: High harmonic spectra generated using our Ti:Sapph + HCF source. With a properly compressed pulse, one can clearly see the effect of gating (blue curve) versus not gating (red curve). The spectra were collected with an electron spectrometer. The electrons were generated by a single-photon absorption in Ar. To recover the EUV energy, one must add 15.76 eV, the ionization potential of Ar.

Knowing that any successful experiment would require a stable source of EUV photons for potentially hours-long experiments, we found it necessary to use both active and passive stabilization techniques. To avoid fast pointing fluctuations, the entire beam line was enclosed. Furthermore, it was critical to stabilize the beam pointing into the HCF to avoid fluctuations in both intensity and central wavelength. The second aspect is especially critical for high harmonic generation, where even a slight shift in central wavelength of the drive beam would lead to a significant central energy shift in the generated harmonics. In the end we were able to obtain pointing stabilization to within 5 μm RMS in X and Y, and a timing jitter of less than 70 as RMS

over hours of operation. To demonstrate this stability, Fig. 2 shows the stability of a gated spectrum over 25 minutes of operation.

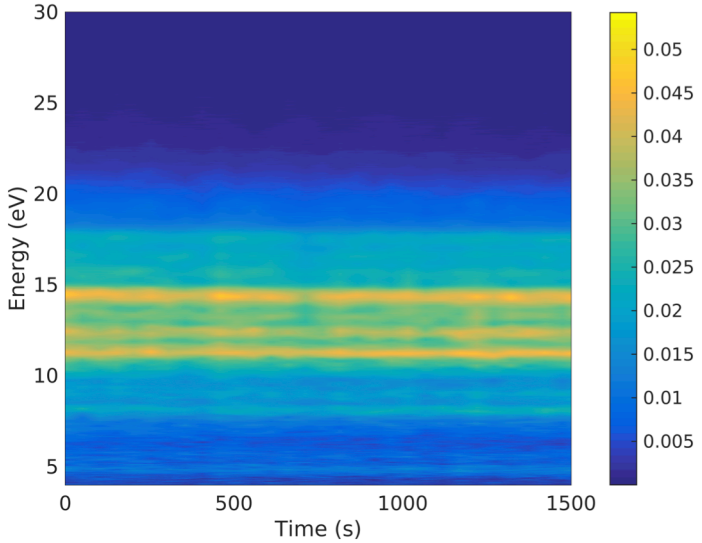

Fig. II.2: Harmonic generation stability study showing negligible energy and intensity drifts of the HHG over a 25 min period after pointing stabilization into the HCF. The spectra are again electron spectra using Ar gas as the target.

With the successful generation of harmonics using our gated 800 nm driver, we then sought to optimize high harmonic efficiency in the 16-18 eV range. Efficiently generating harmonics in this range is difficult with standard atomic gases as their ionization potentials are relatively large. For instance, Kr and Xe have the lowest ionization potentials of ~14 eV and 12.13 eV respectively. By simply increasing the laser intensity to achieve sufficient ionization for HHG, one easily generates photons exceeding 18 eV. One could use filters to isolate the energies between 16-18 eV, but in our experience it was difficult to find the proper response curve with adequate transmission. One last issue with Kr and Xe is their prohibitive cost. In the end, we found we could match or beat the efficiency of Kr and Xe in the 16-18 eV range by simply using molecular gases with lower ionization potentials.

Having an ionization potential of 9.69 eV, acetone gas presented an ideal candidate for low energy harmonic generation. With Acetone gas we could achieve HHG spectra spanning from the 7^{th} to the 11^{th} harmonic (central energies from 10.85-17.05 eV). As we only desired the 11^{th} harmonic, the simplest method to suppress the 7^{th} and 9^{th} harmonics was to use the thinnest possible film of aluminum (typically ranging between 100-250 nm). Finally, to generate the shortest pulse possible, we found that we could increase the 11^{th} harmonic bandwidth using our polarization gating setup. Our final engineered pulse is shown in Fig. II.3 below.

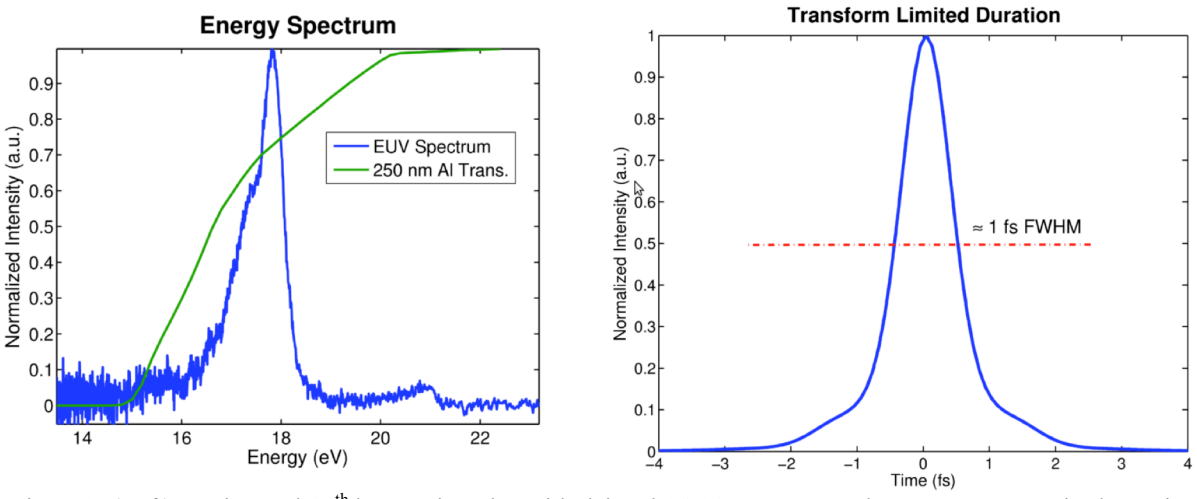

Fig. II.3: (Left) Engineered 11th harmonic pulse with deisred 16-18 eV range. The EUV spectrum is shown in blue, while the green curve demonstrates the transmission of a 250 nm thick Al filter. (Right) The transform limited pulse profile using the experimental spectrum. There is enough generated bandwidth to support pulses down to 1 fs in duration, adequate for measuring dissociation dynamics of H_2 molecules.

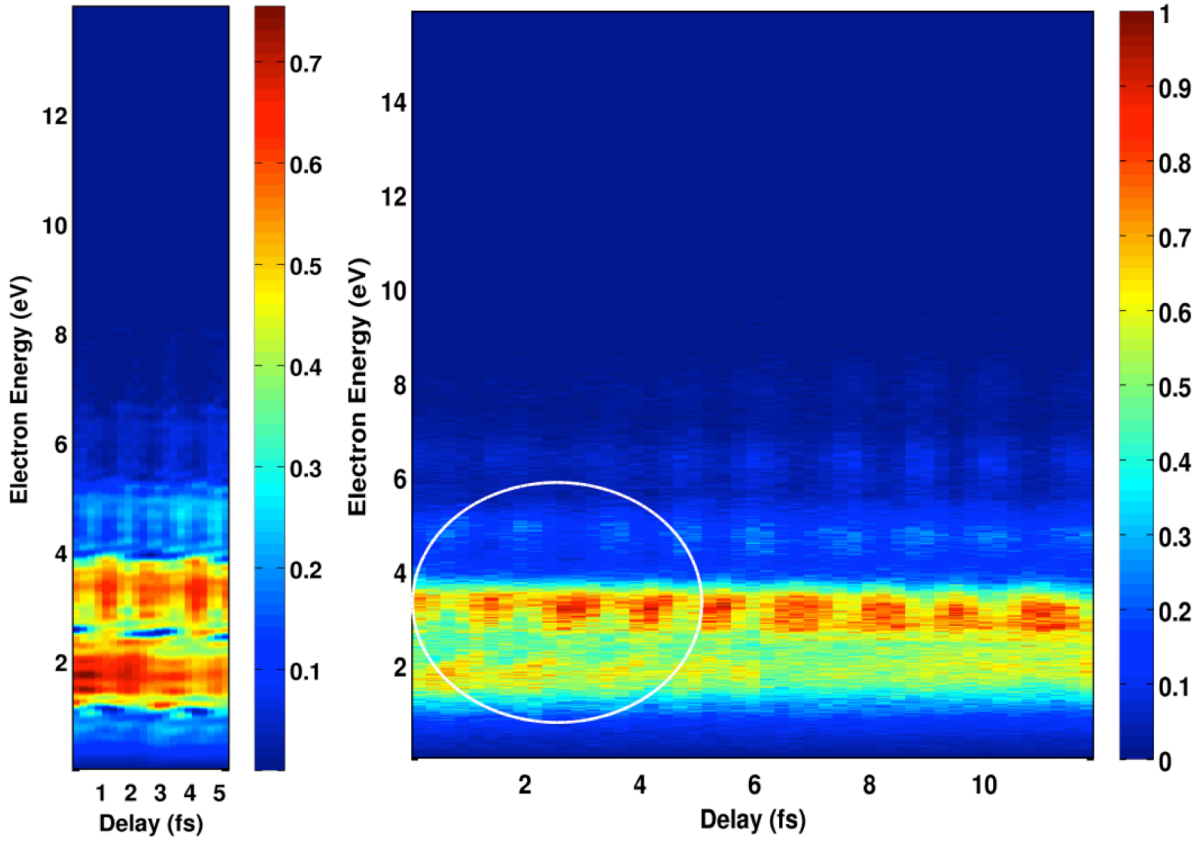

Fig. II.4: (Left) Retrieved spectrogram. (Right) Measured spectrogram. The harmonic spectrum was streaked using a portion of the 8 fs drive pulse from the Ti:Sapph + HCF. The streaking target used was Ar. The circled region indicates the region over which the fit shown on the left was performed.

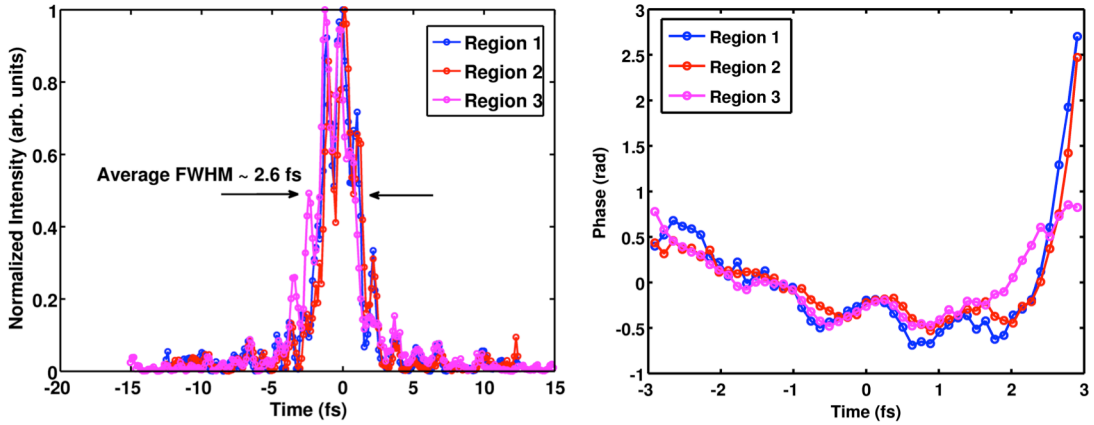

Fig. II.5: (Left) Retrieved pulse envelope (intensity). (Right) Pulse envelope phase. The three curves were obtained from three separate regions of the spectrogram. The average FWHM pulse duration was found to be 2.6 fs, which corresponds to roughly one cycle of the driving IR pulse.

To characterize the temporal duration of the EUV pulse, we used a variation of the FROG-CRAB method that we developed known as the Volkov Transform Generalized Projection Algorithm [2]. This method was developed in order to accommodate several deficiencies of the standard FROG-CRAB approach, and is discussed in more detail in the next section. The results of the pulse characterization are shown in Figs. II.4 and II.5. The results indicate that the pulse duration has been isolated to within one cycle of the driving field (<2.66 fs). To give further confidence to the retrieved pulse form, we fit several separate portions of the retrieved spectrogram, all of which yielded very similar results, and are shown in Fig. II.5.

In conclusion, we were able to engineer an isolated pulse with a bandwidth spanning 16-18 eV, having a pulse duration of 2.66 fs. While the photon energy and pulse duration of these pulses are suitable for studying dynamics of H_2 dissociation in the presence of mid-IR laser fields, the major limiting factor was the EUV flux. The experimental spectrogram in Fig. II.4 took 6 hours to record. When accounting for expected yields of H_2^+ and H^+ during a dissociation experiment, we concluded that at the current flux levels, the measurement time would be as long as several days. With this, it was concluded that to successfully translate these results to realistic experimental conditions using the mid-IR sources needed for the dissociation experiment, an upgrade to higher repetition rates (>10 kHz) would be necessary.

B. Improvements to Attosecond EUV Pulse Characterization

When thinking of how to best characterize the temporal duration of our low-energy HHG pulses, we found that there was clear room for improvement of the standard FROG-CRAB algorithm used for EUV pulse retrieval. Standard versions of this method suffer from the central momentum approximation, which is a well-documented issue [3,4]. Beyond this, there is no natural way for typical FROG techniques to account for the dipole transition matrix element (DTME) of the ionized atom. The latter can be especially important when characterizing low energy harmonics with relatively large bandwidths as the DTME of atomic targets becomes more dispersive as photon energies approach the ionization potential.

Both the central momentum approximation and inability to account for the DTME stem from the fact that standard FROG algorithms are not designed to account for non-separable

functions of momentum and time. While the PROOF [3] algorithm shows a way one could avoid the central momentum approximation, and iPROOF [5] completes a full generalization of the RABBIT technique for an arbitrary spectrum while incorporating physics of the photionization process, these methods are limited to streaking fields that are within the perturbative intensity regime, and are restricted to streaking pulse durations that satisfy the slowly varying envelope approximation. This limits their effectiveness at simultaneously characterizing attosecond pulses along with the complex, broadband electric field waveforms that likely accompany them in streaking measurements [6].

We developed a new reconstruction algorithm for FROG-CRAB, entitled the "Volkov Transform" Generalized Projections Algorithm (VTGPA). Rather than requiring that the minimization step of the reconstruction occur in the time domain form of the spectrogram, it is performed directly in the frequency domain. Using a numerically integrated form of the full expression describing the electron spectrum in the context of the strong field approximation (SFA),

$$P(k,\tau) = \left| \int_{-\infty}^{\infty} \mathrm{d}t\, \mathcal{E}_X(t-\tau) d^{CV}\big(k + A(t)\big) \exp\{i(S(k,t) + I_P t)\} \right|^2 , (1)$$

where k is the final momentum, τ the delay between the IR and attosecond EUV pulse, $\mathcal{E}_X$ the electric field of the attosecond pulse, $A(t)$ the vector potential of the streaking pulse, $d(k)$ the dipole transition matrix element (DTME), and $S(k,t) = \int^t \mathrm{d}t'(k + A(t'))^2$is the accumulated Volkov phase, we show that the electric of the attosecond pulse can be solved for directly in a least squares sense. By solving the expression in the frequency domain, no Fourier transforms steps are needed, making the central momentum approximation unnecessary. As a result, there is no bandwidth limitation, the full form of the DTME can be accounted for, and there is no fundamental constraint on the form of the vector potential so long as Equation (1) is a valid representation of the streaking process.

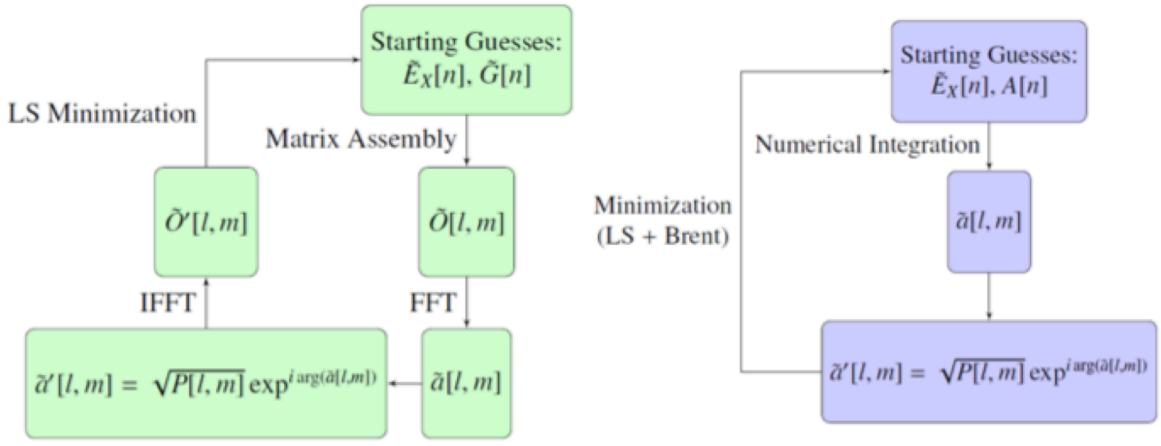

Fig. II.6 (Left) A flowchart of the LSGPA algorithm. In LSGPA, the complex gate function is used to represent the phase gate created by the laser-induced action after applying the central momentum approximation. (Right) A flowchart of the VTGPA algorithm. The flowchart has fewer elements than other GPA approaches, but more computation is being performed in the minimization step. No FFTs are used, and the minimization is performed directly in the frequency domain.

To solve for the vector potential, a more direct fitting approach was taken. To start, $A(t)$ is decomposed into a carrier and envelope. The envelope is formed by creating a cubic spline

between anchor points, and the carrier is represented as $\cos(\omega_0 + \omega_1 t + \omega_2 t^2 \ldots)$, where each ω_n and anchor point is fit using a Brent's method for bounded minimization. A bounded minimization scheme was preferred as in any attosecond streaking experiment, the experimental bounds for the streaking pulse (such as estimated duration and intensity) are easy to measure.

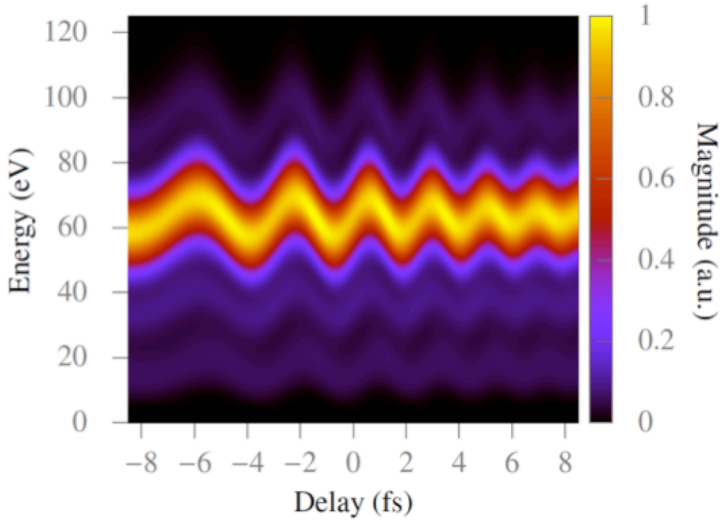

Fig. II.7 Simulated spectrogram used for testing the reconstruction. An attosecond EUV pulse with a cosine squared profile in the energy domain was used. Its bandwidth was set to 120 eV with a central energy of 80 eV, and a group delay dispersion of -2.17×10^{-3} fs². A small side-lobe pulse was included, having the same profile, but with a bandwidth of 100 eV, the same chirp, a time separation of 100 as, and roughly 1/4 peak electric field magnitude. For the IR streaking pulse, a center wavelength of 800 nm, and a Gaussian envelope with duration of 10 fs full width at half maximum (FWHM) in intensity, a linear chirp of 25.5×10^{-3} fs², and a peak intensity of 1×10^{12} W/cm² was used. The target gas was modeled using simulation data for the DTME of Ar.

We have extensively compared VTGPA to a state of the art FROG-CRAB retrieval routine, known as the Least Squares Generalized Projections Algorithm (LSGPA). The flow charts of these two algorithms are shown in Fig. II.6, and the results of both methods using simulated data are shown in Figs. II.7 and II.8. Due to the central momentum approximation, and the fact that it cannot account for the DTME, the LSGPA result is clearly corrupted, while the VTGPA algorithm correctly retrieves the exact pulse form. Furthermore, the VTGPA is also more accurate at retrieving the exact IR waveform. This work has already been presented at two conferences [7,8], and has been submitted for publication [2].

III. 5-micron pulse generation

Significant progress was made toward our goals of generating energetic few-optical cycle pulses in the mid-IR range, including the generation of a 10-fs pulse centered at 2.6 μm (only 1.1 optical cycles) with 1.5 μJ energy (>200MW peak power) with tunable spectral amplitude/phase, and the generation of a 35 fs pulse centered at 6 μm (1.5 optical cycles) with 10 μJ energy (>500MW peak power). The generation of these pulses represents significant advancements in the state of the art, and necessitated significant engineering advancements. For the generation of the 2.6 μm pulse a new conversion technique was used (the first demonstration of such a technique to generate an ultra-broadband pulse), and for the 6 μm pulse a new optical material—

$CdSiP_2$—was used (the first demonstration this material being used to generate pulses of this short a duration and high an energy).

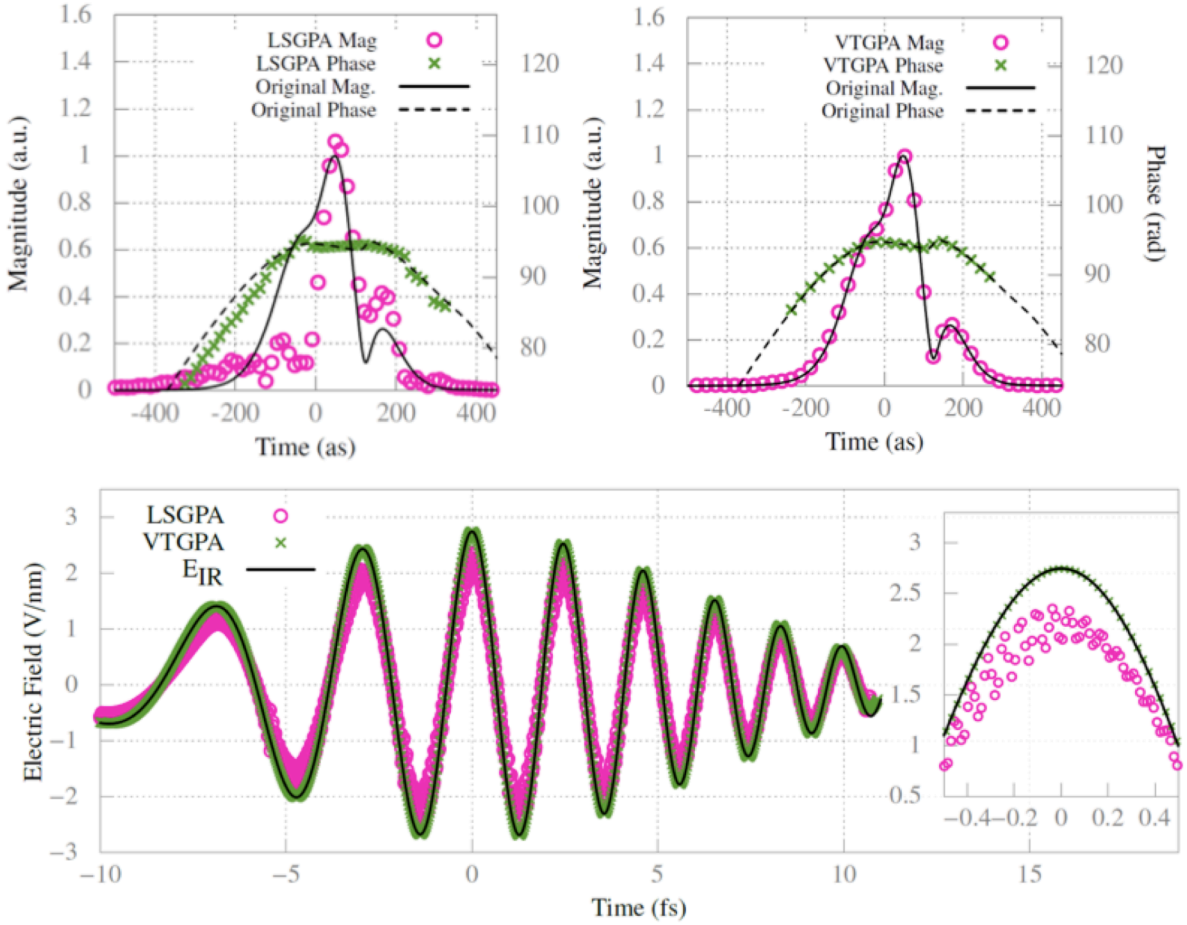

Fig. II.8 (Top left) LSGPA retrieval of the attosecond pulse. As others have observed [3,4,6], the algorithm retrieves a pulse much shorter than the actual value, in this case roughly 50% of the actual FWHM. While the side lobe location is correct, the side lobe intensity is incorrectly retrieved. (Top right) VTGPA retrieval of the attosecond pulse. (Bottom) Comparison of the IR field retrieval using both algorithms. While LSGPA correctly retrives the shape of the IR field, the peak field strength is underestimated, as noted in [4]. Also, since it fits every point independently, the differentiation step needed to convert vector potential to field increases the noise of the retrieval. However, the VTGPA retrieval fits the vector potential with a smooth function, and does not suffer from this noise.

The 2.6 μm pulses were generated via chirped-pulse difference frequency generation (CPDFG) between 2 frequency bands of an amplified Ti:Sapphire laser system. One of the bands was a 0.2 nm bandwidth centered at 1047 nm, which was amplified in a home built Nd:YLF based chirped pulse amplification (CPA) laser system. The other band was a 200nm bandwidth centered at 750 nm which was amplified in a home built optical parametric chirped pulse amplifier (OPCPA) system, which was pumped by the previously mentioned CPA. The difference frequency between these two bands spans from 1.8-4.5 μm, however at the time this project began there was no way to reasonable (even >1%) conversion efficiency over this broad a bandwidth in this wavelength region. To combat this issue a new technique was developed in

collaboration with H. Suchowski, which we call adiabatic frequency generation. This technique takes advantage of the fact that in periodically polled nonlinear crystals (KTP, CLN, etc) it is possible to vary the phase matching conditions along the longitudinal (propagation) axis of the crystal, which allows for one to artificially increase the bandwidth of the phase matching process.

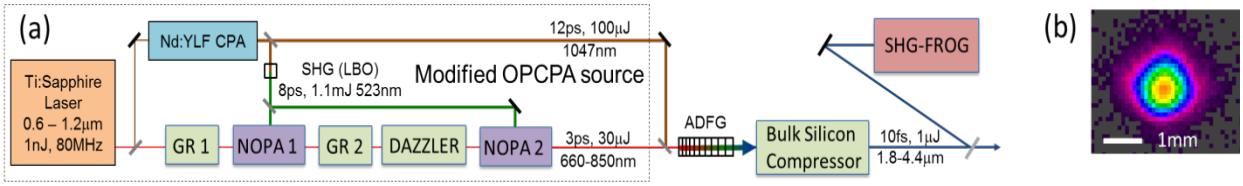

Fig. III.1. (a) Experimental setup: Nd:YLF CPA, 12-ps, 1-kHz, 4-mJ; GR1, grism; NOPA1, BBO 5mm; GR2 grism; Dazzler (Fastlite); NOPA2, BBO 3mm; ADFG, aperiodically poled, 20-mm MgO-doped congruent $LiNbO_3$ grating; Compressor, Bulk Silicon Compressor, 21mm single pass. (b) Far field profile of compressed beam. From ultrafast phenomena submission; to be published in conference proceedings (2016).

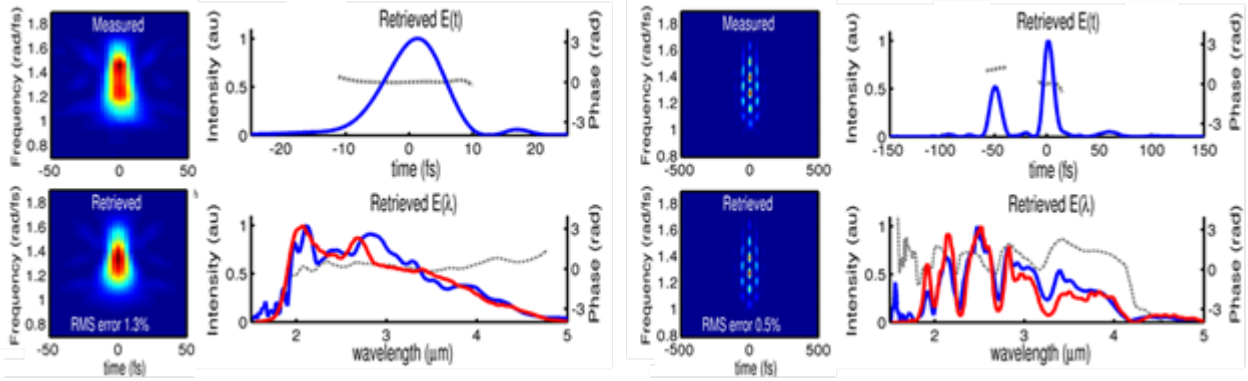

Fig. III.B. (a-d) Experimentally measured FROG characterization of compressed pulse: (a) Measured FROG trace. (b) Retrieved FROG trace. (c) Retrieved electric field in the temporal domain (blue: intensity, gray: phase). (d) Retrieved FROG trace in the spectral domain (blue: retrieved intensity, red: measured intensity; gray: phase). (e-h) Experimentally measured FROG characterization of a pulse pair with 50 fs separation: (e) Measured FROG trace. (f) Retrieved FROG trace. (g) Retrieved electric field in the temporal domain (blue: intensity, gray: phase). (h) Retrieved FROG trace in the spectral domain (blue: retrieved intensity, red: measured intensity; gray: phase). From ultrafast phenomena submission; not yet published.

In this work we used a specific case of adiabatic difference frequency generation whereby the lower energy of the two input bands (the 1047nm band in this case) is much stronger than the other, which results in a situation whereby the conversion to the difference frequency asymptotically approaches unity as the intensity of the middle energy pulse is increased. Furthermore, within the practical limitations of the experiment (achievable poling periods, crystal dimensions, crystal damage threshold, availability of laser sources, etc) we were able to generate an idler spanning from 1.8-4.5 μm with 1.5 μJ energy [9]. Furthermore, an intrinsic property of CPDFG is that many of the properties of the seed pulses are transferred to the generated difference frequency signal, which we use to allow us to shape the generated pulses in the mid-IR using the pulse shaping tools in the near-IR OPCPA system [10]. For example, we used the acousto-optical programmable dispersive filter (AOPDF) in the near-IR

OPCPA system to fine tune the spectral phase on the mid-IR pulse so that we can compress the pulse down to within 15% of its Fourier limited pulse duration of 10 fs using a simple piece of bulk material (Silicon, 21mm in length) [11]. Furthermore, we can further shape the generated mid-IR pulse using the near-IR pulse shaper, for example to generate pulse pairs as may be necessary in pump-probe and spectroscopic measurements [12]. We also point out that the ability to shape the greater-than-octave-spanning bandwidth of the generated mid-IR pulse is not easily achieved using existing pulse shaping techniques (AOPDFs, spatial light modulators inserted in a grating stretcher, and similar devices), which are typically limited to sub-octave bandwidths. Details of the experimental setup are shown in Fig. III.1, and a measurement of the generated mid-IR pulse is shown in Fig. III.2. Complete details of the theoretical modeling and experimental work are given in our publications on the subject [9-12].

The generation of 6 μm pulses is based on traditional optical parametric amplification (OPA). The generated pulse from the aforementioned CPDFG system is combined with a portion of the energy from the 2 μm OPCPA laser system constructed as a part of the pulse synthesizer. The bandwidth of the seed pulse was artificially narrowed (using the AOPDF in the system) to span from 3-4.5 μm (and generating a corresponding 35 fs pulse at 3.6 μm) to match the gain bandwidth of the OPA. Approximately 1 mJ of energy from the pump laser (30 fs in duration at 2.1 μm central wavelength) was used as a pump. These two beams were combined in a nondispersive polarizing beam splitter (consisting of a thin, uncoated, silicon plate at brewsters angle) and the beams were focused onto the OPA crystal. For this work two materials were used, a 1.1 mm thick CSP and 0.5mm thick ZGP crystal, both provided by our collaborator P. Schunemann. Both of these materials were found to work acceptably, with ZGP offering slightly shorter pulse durations and CSP offering slightly higher conversion efficiency. With ZGP an energy of 5 μJ was achieved with a pulse duration of roughly 34 fs (1.7 optical cycles at the 6 μm central wavelength), and with CSP and energy of 10 μm as achieved with a pulse duration of roughly 40fs. The duration of the pulses were characterized in a homebuilt interferometric autocorrelator, and are roughly compressed as shown in Figure C. Complete details of the theoretical modeling and experimental work are given in our publications on the subject [13-14].

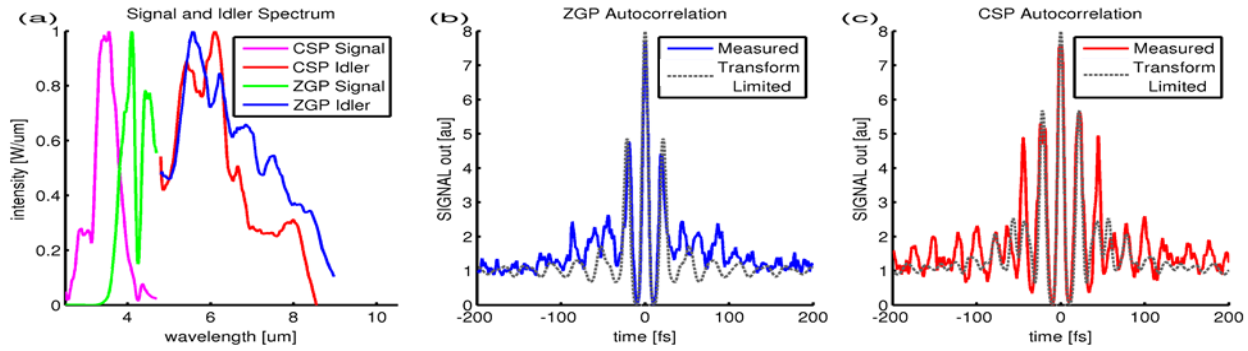

Fig. III.3 (a) Measured amplified spectra of signal and idler with ZGP crystal and CSP crystal. (b) Measured autocorrelation of ZGP idler (blue) and transform limited autocorrelation (grey, 32 fs FWHM). (c) Measured autocorrelation of CSP idler (red) and transform limited autocorrelation (grey, 33 fs FWHM).

IV. Multiplexed laser system development

Significant progress was made toward our goals of improving the laser facilities to support the needs of the experiments proposed for this project, including significant improvements to the existing pulse synthesizer system to improve its long-term stability, a complete overhaul of the high power pump laser system to improve its energy and stability, and the construction of additional OPCPA amplifier stages to amplify the output of the existing pulse synthesizer to the millijoule levels. The net result of these efforts include a novel hybrid room temperature Yb:KGW / cryogenically cooled Yb:YAG pump laser system capable of delivering 50 mJ pulses compressed to 6 ps duration, and a pulse synthesizer capable of generating pulses CEP stable pulses at 800 nm and 2.1 μm with 0.6 mJ and 0.3 mJ pulse energies, respectively, with pulse durations of 10 fs and 21 fs respectively, and with sufficient stability for the experiments proposed. At the time of construction the pump laser was the most energetic cryogenically cooled picosecond laser system operating a kilohertz repetition rates, and the unique capability of the pulse synthesizer to generate highly intense, multi-color, pulses synchronized with sub-femtosecond resolution was unmatched.

The basis for the work on this project was the pulse synthesizer already constructed at MIT by the Kaertner group [15]. To meet the demands of this project it was necessary to improve both the long term stability of the system (the existing system needed frequency re-alignment, and the experiments proposed require many hours of uninterrupted operation) and the output energy (the existing system produced 20 μJ in each color, these experiments require in excess of 500 μJ in the near-IR arm and roughly 100 μJ in the mid-IR arm). After a careful study of the existing laser system it was determined that the primary source of instabilities was the pump laser system (which consists of a home built Nd:YLF CPA laser system), and in particular while the pulse energy of this system was highly stable there were slight changes in the output pointing of the beam which caused the performance of the following OPCPA stages to degrade over the course of several hours. This was solved by adding a semi-custom beam pointing stabilization system which used quadrant photodiode detectors and piezo-electric actuated mirrors to remove the slow drifts from the pump laser. The result of this improvement, as shown in Fig. IV.1, was an order of magnitude reduction of beam pointing drifts in the system, from a movement of the center of the beam as measured at the first near-IR OPCPA stage from 0.5 mm over 2 hours to 0.03mm over the same period.

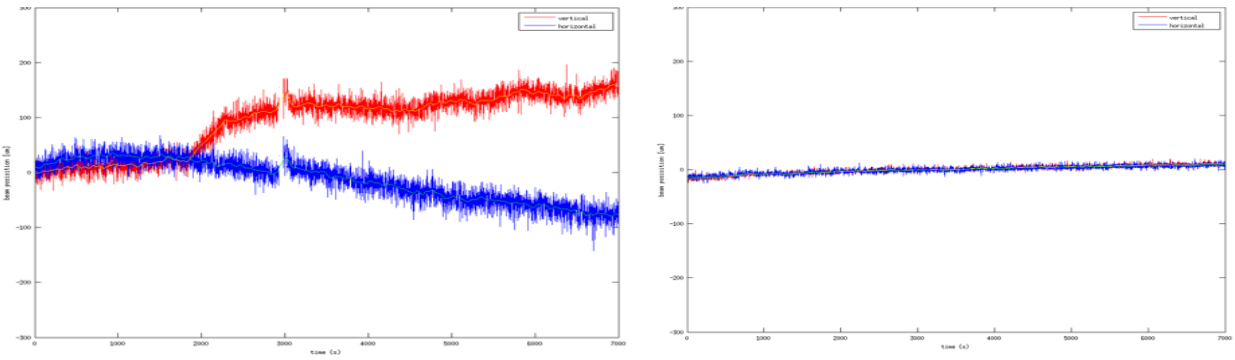

Fig. IV.1: Pointing stability of Nd:YLF pump laser over a 2 hour period without (left) and with (right) the active pointing stabilization active.

This improvement removed the majority of the alignment drift present if the system; however there still remained a slow shift in the central wavelength and output power due to slight timing drifts between the pump laser and OPCPA system, which are a result of slight

thermal fluctuations in the oscillator and regenerative amplifier. Because these drifts were purely thermal drifts it was possible to remove them entirely with a slow feedback loop based on monitoring the spectrum of the amplified pulses in the OPCPA and adjusting a motorized delay line to adjust the optical path length between the pump and seed lasers With these two improvements the OPCPA systems were free of pointing and spectral/power shifts, as shown in Fig. IV.2.

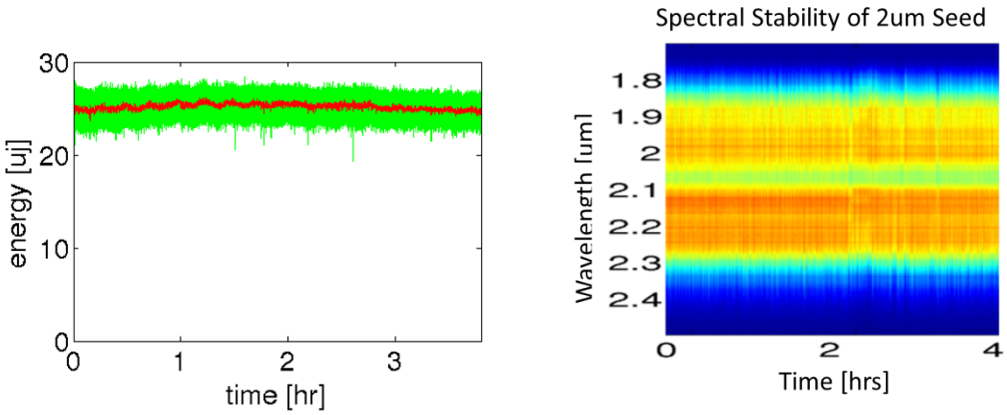

Fig. IV.2: Energy and spectral stability of the 2 μm laser system measured over a 4 hour period. The RMS energy fluctuations were 2.5% RMS over 10 second 2.8% over the full 4 hour period.

Further improvements were required in the 800nm OPCPA system to increase the bandwidth of this amplifier to meet the needs of the proposed experiments. This necessitated an complete rebuild of the 800nm OPCPA system, including the replacement of the original prism based stretcher with a prism+grating 'grism' stretcher, reduction of thickness of the amplifier crystals, and careful attention to optimizing the system for a broad bandwidth while maintaining keeping the beam profile, energy, superfluorescence, etc., at acceptable levels [9]. The improvement in the bandwidth achievable in the 800nm arm of the pulse synthesizer is shown in Fig. IV.3, and the new system supports the generation of pulses as short as 7 fs in duration.

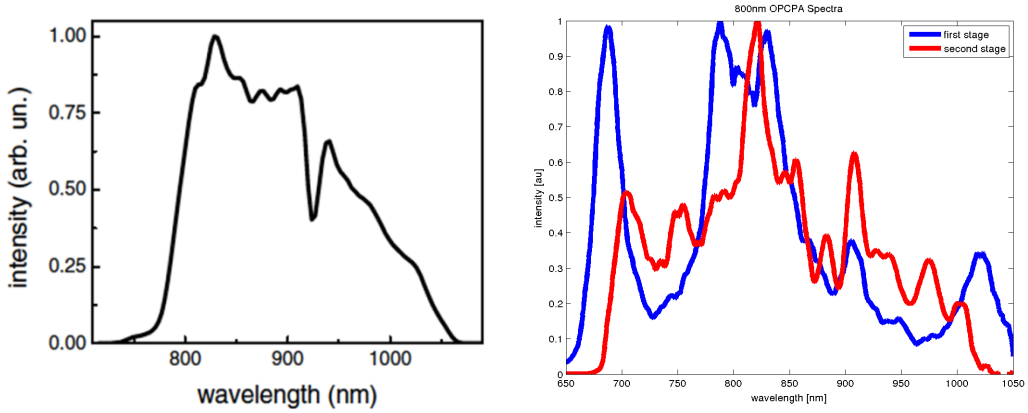

Fig. IV.3: Measured spectrum of the 800nm laser system before (left) and after (right) being rebuilt. The spectral narrowing from 1st(blue) to 2nd (red) stage is due to the limited bandwidth of the pulse between these stages.

After the upgrades to the pulse synthesizer seed system were completed it was possible to add the additional power amplifiers needed to amplify the ~10 μJ energies available from the seed system to the millijoule levels needed for the proposed experiments. In the 800nm channel an additional amplifier consisting of a 2mm thick BBO crystal was used, which was pumped by up to 8 mJ at 523nm (provided by the cryogenic pump laser system discussed later), to produce up to 0.6 mJ at 800nm. As shown in Fig. IV.4 the spectrum after amplification preserves the full bandwidth of the seed signal shown in Fig. IV.3, and the 7 fs transform limited pulse duration was preserved. The 2 μm laser system was amplified in a 1.8mm thick periodically polled SLT crystal using up to 5 mJ pulse energy at 1030nm (also provided by the cryogenic pump laser) to achieve up to 0.3 mJ amplified pulse energy. As shown in Fig. IV.4, the bandwidth from the seed source was again preserved and the amplified spectrum supports a 21-fs pulse duration. Inherent to the OPCPA based pulse synthesizer architecture is the fact that the pulses could easily be recompressed using the existing compressors, only requiring minor corrections to integrated pulse shapers to compensate for the dispersion of the added components. In addition to the SLT based 2 μm amplifier, an additional amplifier consisting of a 5-mm thick BBO crystal was used to achieve energies at high at 3.5 mJ using up to 50 mJ at 1030nm (from the cryogenic pump laser), with a narrower bandwidth corresponding to a 30 fs pulse duration, which was used for powering the further mid-IR OPA used to generate pulses at 6 μm, as discussed in detail elsewhere.

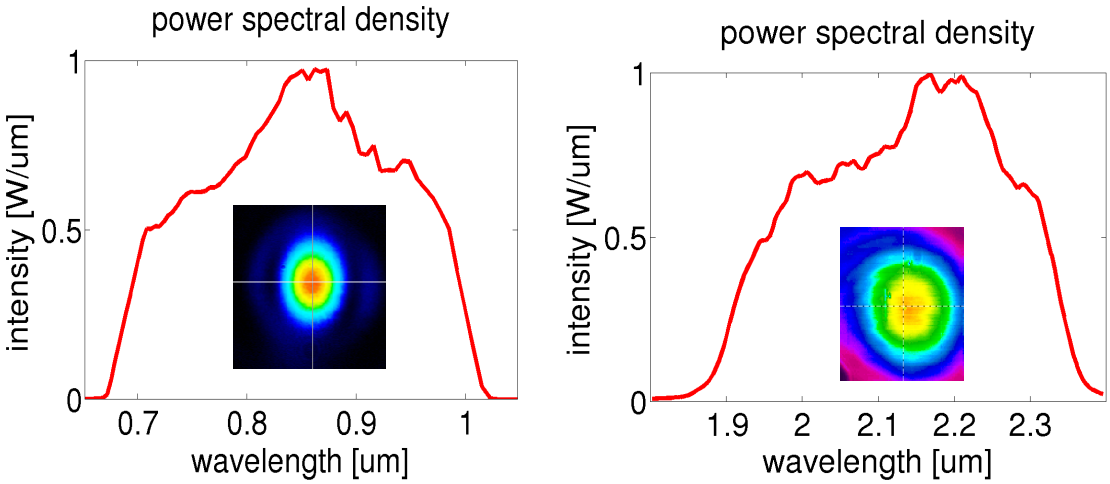

Fig. IV.4: Measured spectrum of the 800nm laser system (left) and 2 μm laser system (right) after amplification in the final stage. The measured beam profiles of each system are shown in the insets.

In addition to the OPCPA upgrades, the cryogenic pump laser system required a complete overhaul to achieve the performance needed for the goals set forth in this project. After a careful study of the performance of the existing cryogenic pump laser system at MIT, it was concluded that the primary source of instabilities in the system was the home-built cryogenically cooled regenerative amplifier, which had issues relating to thermal drifts in the system causing pointing shifts and the being prone to bi-stable operation due to the lifetime of cryogenic Yb:YAG being relatively close to the repetition rate of the system. Both of these issues were eliminated by moving to a commercial Yb:YGW regenerative amplifier, at the expense of greatly reduced output power (2 mJ compared to the nearly 10 mJ available from the home-built system). The reduced output power of the regenerative amplifier was compensated for by increasing the gain

in the multipass amplifier chain, and furthermore the increased bandwidth available from the Yb:KGW amplifier (greater than 0.5nm compared to the ~0.1nm available with the cryogenic amplifier) increased the stretched pulse duration throughout the amplifier chain, and reduced the nonlinear phase (B-integral) accumulated in the multipass amplifier. The design of the complete amplifier system is discussed at length in our publications [16,17]. Furthermore, the increased bandwidth allowed the generation of shorter compressed pulses (8 ps compared to 18 ps available previously), which simplified the dispersion management throughout the OPCPA system. Fig. IV.5 shows an autocorrelation of the compressed pulses and the beam profile of the amplified beam.

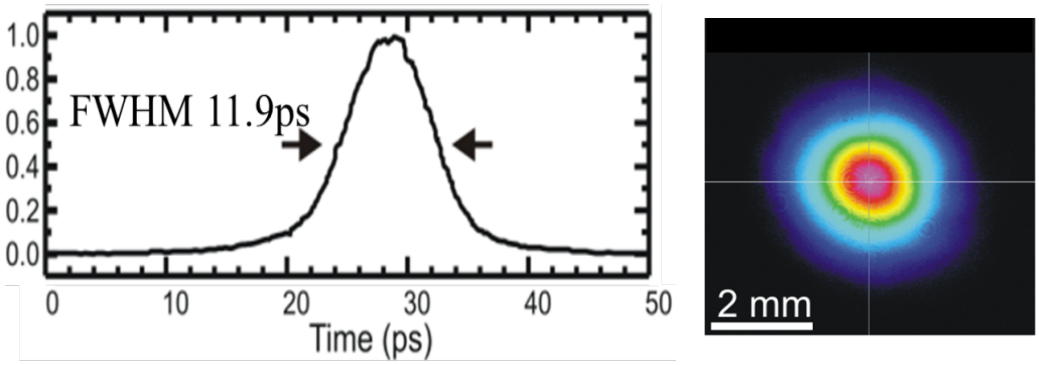

Fig. IV.5: Left - Autocorrelation of the compressed 1030nm pulses, assuming a Sec^2 pulse the deconvolved pulse duration is 8.2 ps. Right – Measured beam profile of the amplified beam.

After the upgrades to the seed system and multipass amplifier it was concluded that the pointing fluctuations (introduced due to thermal drifts of the optical table upon which the amplifier was built) were too large for stable OPCPA operation, so an additional pointing stabilizer was added which reduced the pointing fluctuations to negligible levels, as shown in Fig. IV.6. Also shown in Fig. IV.6 is the energy stability of the system, which was measured to be 1% RMS over 10 seconds and 3.5% RMS over an 8 hour period.

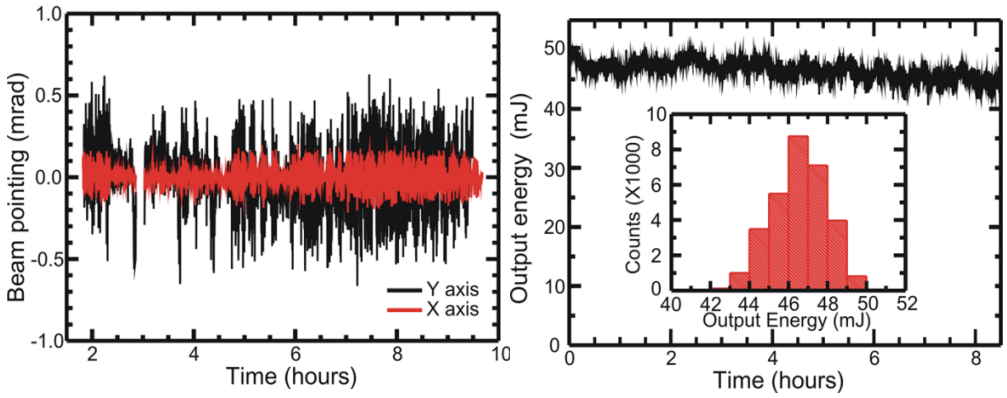

Fig. IV.6: Pointing and energy stability of the compressed beam. Left – Pointing stability of the system with the pointing stabilizer active, the pointing drifts are 6 μRad in the horizontal and 2 μRad in the vertical direction. Right – Energy stability of the system, showing a 1% RMS fluctuation over a 10 s measurement period, and 3.5% RMS over the full 8 hour period. The inset shows the pulse energy distribution over the first 60 seconds of the measurement.

References

[1] S. Carbajo, et al., Opt. Lett. 39, 2487-2490 (2014).
[2] P. D. Keathley, et al., *New J. of Physics (Submitted)*.
[3] M. Chini, et al., Optics Express 18 12, 13006– 13016 (2010).
[4] J. Gagnon, et al., Appl. Phys. B 92, 25–32 (2008).
[5] G. Laurent, et al., Optics Express 21 14, 16914– 16927 (2013).
[6] A. Wirth, et al., Science 334 195–200 (2011).
[7] P. D. Keathley, et al., *UFO 2015*, UFO0138, (2015).
[8] P. D. Keathley, et al., *CLEO 2015*, JW2A.35. (2015).
[9] H. Suchowski, et al., *Opt. Express* 21, 28892-28901 (2013).
[10] P. R. Krogen, et al., *Ultrafast Phenomena 2014*, paper 08.Tue.D.6 (2014).
[11] P. Krogen, et al., *Ultrafast Phenomena 2016*, paper UTu2A.1 (2016).
[12] P. Krogen, et al., *CLEO 2015*, SW1O.3. (2015).
[13] H. K. Liang, et al., *High-Brightness Sources and Light-Driven Interactions*, paper MS4C.1 (2016).
[14] P. Krogen, et al., *CLEO 2016*, paper STu3I.4 (2016).
[15] S.W. Huang, et al., *Nat. Photon.* 5, 475 (2011).
[16] C.-L. Chang, et al., *Opt. Express* 23, 10132 (2015).
[17] C.-J. Lai, et al., *J. Opt.* 17, 094009 (2015).

1.

1. Report Type

Final Report

Primary Contact E-mail
Contact email if there is a problem with the report.

moses@cornell.edu

Primary Contact Phone Number
Contact phone number if there is a problem with the report

607-255-6704

Organization / Institution name

Cornell University/MIT

Grant/Contract Title
The full title of the funded effort.

Phase-sensitive control of molecular dissociation through attosecond pump/strong-field mid-IR probe spectroscopy

Grant/Contract Number
AFOSR assigned control number. It must begin with "FA9550" or "F49620" or "FA2386".

FA9550-12-1-0080

Principal Investigator Name
The full name of the principal investigator on the grant or contract.

Jeffrey Moses/Franz Kaertner

Program Manager
The AFOSR Program Manager currently assigned to the award

Enrique Parra

Reporting Period Start Date

04/01/2012

Reporting Period End Date

11/30/2015

Abstract

The overarching goal of our program was to develop a novel laser and ion spectroscopy system and to use it for the study of strong-field light-matter interactions in the H2 molecule, with molecular ionization and dissociation timed precisely by means of synchronized few-fs EUV and few-cycle mid-IR pulses. This scheme is predicted to allow synchronization of a bound vibrational wavepacket oscillation cycle with a mid-IR electromagnetic field cycle. While our laser system came up short in the EUV flux required to study the dissociation physics of the H2 molecule in the two-color pulse scheme (upgrade to a laser repetition rate of ≥ 10 kHz will be necessary), our efforts produced advances, some major, in several core technologies that can be used for such experiments in the future. These technologies include

Two-color driven (EUV/mid-IR) ion spectroscopy: we designed an interferometer combining EUV and mid-IR light pulses, stable to within a fraction of the mid-IR light field period, with a H2 molecular gas target at the aperture of an ion time-of-flight (TOF) spectrometer for molecular ion spectroscopy, an electron time-of-flight (TOF) spectrometer for attosecond pulse characterization, and an EUV spectrometer for EUV light pulse spectral characterization, all accessible while the system remains under vacuum.

Low photon energy (16-18 eV) isolated single-femtosecond EUV pulse generation: combining the use of low ionization threshold gas, an annual near-IR drive beam, polarization gating, and spectral filtering, we engineered a source of isolated EUV light pulses covering the narrow range of frequencies allowing excitation of H2 to bound H2+ with a duration short enough (2.6 fs) to last a fraction of a bound H2+ vibrational wavepacket cycle. This is a first source of isolated EUV pulses in this energy range and at close to transform limited duration, and we expect our results will inform the approaches used by attosecond and photoemission spectroscopy researchers in the future. Furthermore, we improved the FROG-CRAB EUV pulse characterization method by means of a new algorithm allowing increased accuracy that will be valuable generally for attosecond spectroscopy, especially in the low-photon energy range, where the state-of-the-art approach can be plagued by significant systematic errors.

Few-cycle, intense, 2.6- and 6-micron mid-IR pulse generation: combining a novel nonlinear optical approach for coherent octave-spanning mid-IR seed pulse generation (adiabatic frequency conversion) with novel nonlinear optical materials for mid-IR OPA (ZGP and CSP), and using our few-cycle 2-micron pulse source as the OPA pump, we demonstrated octave-spanning intense mid-IR pulses centered in the 5-6 micron range. These pulses can drive strong-field dissociation synchronized to the vibrational frequency of H2+. The technologies demonstrated here are major advances that will boost strong-field physics in the mid-IR range, an area of current interest by the AFOSR and DoD.

High-energy coherent synthesis of few-cycle near-IR and mid-IR light pulse sources: Using a cryo-Yb:YAG picoseond pump laser we scaled both 800-nm and 2-micron OPCPA systems in our pulse synthesizer to produce few-cycle, sub-mJ-energy pulses. These pulses can be coherently locked by means of the coherent wavelength multiplexing method to within a small fraction of the mid-IR optical period. We improved the picoseond cryo-Yb:YAG laser amplifier technology to be superior in stability, duration, and pulse energy. These improvements to OPCPA technology are major advances for the field.

Together, these technologies represent a significant step forward for attosecond and strong-field spectroscopy, employing a laser technology suitable for high average power and precisely shaped two-color pulse sequences to be used for control of atoms and molecules along both electronic and vibrational degrees of freedom.

Distribution Statement

This is block 12 on the SF298 form.

Distribution A - Approved for Public Release

Explanation for Distribution Statement

If this is not approved for public release, please provide a short explanation. E.g., contains proprietary information.

SF298 Form

Please attach your SF298 form. A blank SF298 can be found here. Please do not password protect or secure the PDF The maximum file size for an SF298 is 50MB.

FA9550-12-1-0080 AFD-070820-035.pdf

Upload the Report Document. File must be a PDF. Please do not password protect or secure the PDF . The maximum file size for the Report Document is 50MB.

FA9550-12-1-0080 Final Report vFinal.pdf

Upload a Report Document, if any. The maximum file size for the Report Document is 50MB.

Archival Publications (published) during reporting period:

1. K.-H. Hong, C.-J. Lai, V.-M. Gkortsas, S.-W. Huang, J. Moses, E. Granados, S. Bhardwaj, and F. X. Kärtner, "High-harmonic generation in Xe, Kr, and Ar driven by a 2.1-μm source: high-harmonic spectroscopy under macroscopic effects," Phys. Rev. A 86, 043412 (2012).

2. H. Suchowski, P. R. Krogen, S.-W. Huang, F. X. Kärtner, and J. Moses, "Octave-spanning coherent mid-IR generation via adiabatic difference frequency conversion," Opt. Express 21, 28892-28901 (2013).

3. K.-H. Hong, C.-J. Lai, J. Siqueira, P. Krogen, J. Moses, L. C.-L. Chang, G. J. Stein, L. E. Zapata, and F. X. Kärtner "Multi-mJ, kHz, 2.1-µm optical parametric chirped-pulse amplifier and high-flux soft X-ray high-harmonic generation," Opt. Lett. 39, 3145 (2014).

4. S. Carbajo, E. Granados, D. Schimpf, A. Sell, K.-H. Hong, J. Moses, and F. X. Kärtner, "Efficient generation of ultra-intense few-cycle radially polarized laser pulses," Opt. Lett. 39, 2487-2490 (2014).

5. C. Manzoni, O. D. Mücke, G. Cirmi, S. Fang, J. Moses, S.-W. Huang, K.-H. Hong, G. Cerullo, and F. X. Kärtner, "Coherent pulse synthesis: towards sub-cycle optical waveforms," Laser & Photon. Rev. 9, 129 (2015).

6. C.-L. Chang, P. Krogen, H. Liang, G. J. Stein, J. Moses, C.-J. Lai, J. P. Siqueira, L. E. Zapata, F. X. Kärtner, and K.-H. Hong, "Multi-mJ, kHz, ps deep-ultraviolet source," Opt. Lett. 40, 665 (2015).

7. C.-L. Chang, P. Krogen, K.-H. Hong, L. E. Zapata, J. Moses, A.-L. Calendron, H. Liang, C.-J. Lai, G. J. Stein, P. D. Keathley, G. Laurent, and F. X. Kärtner, "High-energy, kHz, picosecond hybrid Yb-doped chirped-pulse amplifier," Opt. Express 23, 10132 (2015).

8. C.-J. Lai, K.-H. Hong, J. P. Siqueira, P. Krogen, C.-L. Chang, G. J. Stein, H. Liang, P. D. Keathley, G. Laurent, J. Moses, L. E. Zapata, and F. X. Kärtner, "Multi-mJ mid-infrared kHz OPCPA and Yb-doped pump lasers for tabletop coherent soft x-ray generation," J. Opt. 17, 094009 (2015).

9. P. D. Keathley, S. Bhardwaj, J. Moses, G. Laurent, and F. Kaertner, "Volkov Transform Generalized Projection Algorithm for Attosecond Pulse Characterization," New J. of Physics (Submitted, 2016).

Changes in research objectives (if any):

In the last year of our grant, we found the flux of our isolated few-fs EUV pulses to be two orders of magnitude too low for spectroscopy experiments that can be conducted within a day. For the remainder of the grant term, we focused on completing the development of an octave-spanning, strong-field, 6-micron-wavelength source that could be used for novel single-color experiments in strong-field H2+ dissociation.

Change in AFOSR Program Manager, if any:

Extensions granted or milestones slipped, if any:

NCE awarded, ending Nov. 30, 2015

AFOSR LRIR Number

LRIR Title

Reporting Period

Laboratory Task Manager

Program Officer

Research Objectives

Technical Summary

Funding Summary by Cost Category (by FY, $K)

	Starting FY	FY+1	FY+2
Salary			
Equipment/Facilities			
Supplies			
Total			

Report Document

Report Document - Text Analysis

Report Document - Text Analysis

Appendix Documents

2. Thank You

E-mail user

Apr 12, 2016 13:39:15 Success: Email Sent to: moses@cornell.edu